BIOCHEMISTRY
including biophysical chemistry & molecular biology
Article

Biochemistry **2010,** *49,* 5891–5898 5891
DOI: 10.1021/bi100782b

Molecular Architecture of a *C*-3′-Methyltransferase Involved in the Biosynthesis of D-Tetronitrose[†,‡]

Nathan A. Bruender,[§] James B. Thoden,[§] Manpreet Kaur,[∥] Marie K. Avey,[∥] and Hazel M. Holden*[,§]

[§]*Department of Biochemistry, University of Wisconsin, Madison, Wisconsin 53706, and*
[∥]*Edgewood Campus Middle School, Madison, Wisconsin 53711*

Received May 18, 2010; Revised Manuscript Received June 8, 2010

ABSTRACT: *S*-Adenosylmethionine (SAM)-dependent methyltransferases are involved in a myriad of biological processes, including signal transduction, chromatin repair, metabolism, and biosyntheses, among others. Here we report the high-resolution structure of a novel *C*-3′-methyltransferase involved in the production of D-tetronitrose, an unusual sugar found attached to the antitumor agent tetrocarcin A or the antibiotic kijanimicin. Specifically, this enzyme, referred to as TcaB9 and cloned from *Micromonospora chalcea*, catalyzes the conversion of dTDP-3-amino-2,3,6-trideoxy-4-keto-D-glucose to dTDP-3-amino-2,3,6-trideoxy-4-keto-3-methyl-D-glucose. For this analysis, two structures were determined to 1.5 Å resolution: one in which the enzyme was crystallized in the presence of SAM and dTMP and the other with the protein complexed to *S*-adenosylhomocysteine and its dTDP-linked sugar product. The overall fold of the monomeric enzyme can be described in terms of three domains. The N-terminal domain harbors the binding site for a zinc ion that is ligated by four cysteines. The middle domain adopts the canonical "SAM-binding" fold with a seven-stranded mixed β-sheet flanked on either side by three α-helices. This domain is responsible for anchoring the SAM cofactor to the protein. Strikingly, the C-terminal domain also contains a seven-stranded β-sheet, and it appears to be related to the middle domain by an approximate 2-fold rotational axis, thus suggesting TcaB9 arose via gene duplication. Key residues involved in sugar binding include His 181, Glu 224, His 225, and Tyr 222. Their possible roles in catalysis are discussed.

Methylation is a common theme in biology where methyl groups are added to the carbons, oxygens, sulfurs, or nitrogens of such molecules as proteins, nucleic acids, phospholipids, sugars, and hormones, among others. The enzymes responsible for these methylation events are termed *C*-, *O*-, *S*-, and *N*-methyltransferases, respectively, and they typically require *S*-adenosylmethionine (SAM)[1] for activity. Thus far, five major structural classes have been identified for SAM-dependent proteins (*1*). By far, the most known fall into the Class I category, and remarkably, they often share very little amino acid sequence identity with each other. Members of the Class I family are characterized by a core of ~150 amino acid residues that fold into a seven-strand mixed β-sheet flanked on either side by α-helices to produce an $\alpha\beta\alpha$ sandwich. The core is somewhat reminiscent of the Rossmann fold for dinucleotide binding. The first three β-strands of the core form the SAM binding domain, whereas the last four β-strands typically provide the platform for substrate binding. In light of the diversity of substrates that are methylated, it is not surprising, however, that the substrate-binding regions vary among the Class I methyltransferases (*2*).

In recent years, a variety of microbial SAM-dependent methyltransferases have been identified that are specifically involved in the biosynthesis of unusual di-, tri-, and tetradeoxy sugars (*3*). These particular carbohydrates, found on natural products such as antibacterial and antitumor agents, are often important for the bioactivities of the compounds to which they are attached. The first biochemical characterization of a sugar *C*-3′-methyltransferase focused on TylC3 from *Streptomyces fradiae*, an enzyme involved in the biosynthesis of L-mycarose (*4*). Since this initial study, the activities of additional *C*-methyltransferases that function on nucleotide-linked sugars have been verified in vitro (*5*, *6*).

Here we report the first three-dimensional structure of a *C*-3′-methyltransferase, namely that from *Micromonospora chalcea* referred to as TcaB9 (*7*). This enzyme is involved in the production of D-tetronitrose (Scheme 1), a tetradeoxy sugar found in the antibacterial and antitumor agent tetrocarcin A (*7*). The sugar itself is appended to the polycyclic aglycone via the action of a glycosyltransferase that requires dTDP-tetronitrose as its substrate (*7*). Note that D-tetronitrose is also referred to in the literature as D-kijanose, which is found on the antibiotic kijanimicin (*8*).

The biosynthesis of dTDP-tetronitrose in *M. chalcea* requires 10 enzymes (*7*). TcaB9 reportedly catalyzes the fifth reaction in the pathway, which involves the transfer of a methyl group from SAM to C-3′ of dTDP-3-amino-2,3,6-trideoxy-4-keto-D-glucose (Scheme 1). For the X-ray analysis presented here, the structures of two ternary complexes were determined: the enzyme crystallized

[†]This research was supported in part by National Science Foundation Grant MCB-0849274 to H.M.H.

[‡]X-ray coordinates have been deposited in the Protein Data Bank of the Research Collaboratory for Structural Bioinformatics, Rutgers University, New Brunswick, NJ (entries 3NDI and 3NDJ).

*To whom correspondence should be addressed. E-mail: Hazel_Holden@biochem.wisc.edu. Fax: (608) 262-1319. Phone: (608) 262-4988.

[1]Abbreviations: DTT, dithiothreitol; ESI, electrospray ionization; HEPES, 4-(2-hydroxyethyl)-1-piperazineethanesulfonic acid; IPTG, isopropyl β-D-thiogalactopyranoside; LB, Luria-Bertani; Ni-NTA, nickel-nitrilotriacetic acid; PCR, polymerase chain reaction; rms, root-mean-square; SAH, *S*-adenosylhomocysteine; SAM, *S*-adenosylmethionine; D-tetronitrose, 2,3,4,6-tetradeoxy-4-(methylcarbamyl)-3-*C*-methyl-3-nitro-D-*xylo*-hexopyranose; TEV, tobacco etch virus; dTMP, 2-deoxythymidine monophosphate; dTDP, 2-deoxythymidine diphosphate; Tris, tris(hydroxymethyl)aminomethane.

Published on Web 06/08/2010

in the presence of SAM and dTMP and the enzyme complexed with *S*-adenosylhomocysteine (SAH) and its dTDP sugar product, dTDP-3-amino-2,3,6-trideoxy-4-keto-3-methyl-D-glucose. The latter structure represents a detailed glimpse of a nucleotide-linked keto sugar bound in an enzyme active site. Our investigation demonstrates that TcaB9 functions as a monomer and belongs to the Class I fold of SAM-dependent proteins. Details concerning the overall molecular architecture of TcaB9 are presented.

MATERIALS AND METHODS

Cloning, Expression, and Purification. *M. chalcea* (NRRL 11289) was obtained from the Agriculture Research Service (ARS) Culture Collection, and genomic DNA was isolated according to standard protocols. The *tcab9* gene was PCR-amplified from genomic DNA using the forward primer 5′-AAAA*CATATG*T-CCCACCTGGCCGACGTCT-3′ and the reverse primer 5′-AAA-A*CTCGAG*TCAGCGGATGTGCACCTCCGG-3′, which added *Nde*I and *Xho*I cloning sites, respectively. The purified PCR product was A-tailed and ligated into a pGEM-T (Promega) vector for blue-white screening and sequencing. A TcaB9-pGEM-T vector construct of the correct sequence was then digested with *Nde*I and *Xho*I, and the *tcab9* gene was ligated into a pET28JT vector (*9*) for production of the protein with a TEV protease cleavable N-terminal hexahistidine tag.

The TcaB9-pET28JT plasmid was used to transform Rosetta 2 (DE3) competent cells (Novagen). The cultures were grown in LB medium supplemented with kanamycin at 37 °C with shaking until optical densities of ~0.6, measured at 600 nm, were reached. The cells were then cooled to 16 °C, and overexpression of TcaB9 was induced with 1 mM IPTG (final concentration). The cells were allowed to express protein at 16 °C for 18 h. TcaB9 was purified at 4 °C following standard procedures using nickel-nitrilotriacetic acid (Ni-NTA) resin (Qiagen). The purified protein was incubated in the presence of 1 mM DTT and TEV protease in a 50:1 (TcaB9:TEV protease) molar ratio at room temperature for 36 h. The TEV protease was subsequently removed via Ni-NTA column chromatography. TEV-cleaved TcaB9 was dialyzed against 20 mM HEPES (pH 7.5) and 100 mM NaCl, concentrated to 25.8 mg/mL on the basis of an extinction coefficient of 0.68 $(mg/mL)^{-1}cm^{-1}$ at 280 nm, and subsequently flash-frozen in liquid nitrogen.

Scheme 1

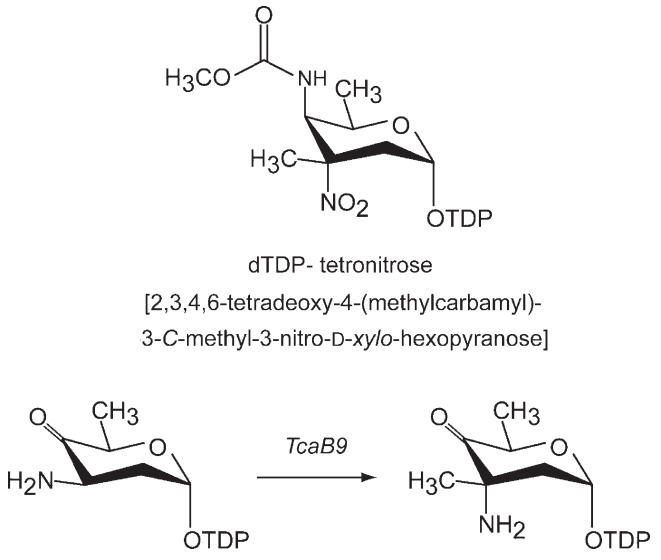

Crystallization of TcaB9. Crystallization conditions were initially surveyed by the hanging drop method of vapor diffusion with a sparse matrix screen developed in the laboratory, using the protein incubated with 10 mM dTDP and 5 mM SAM. Diffraction quality crystals of the TEV-cleaved enzyme were grown by mixing in a 1:1 ratio the enzyme and 1.3−1.5 M sodium/potassium phosphate (pH 8.0). These crystals belonged to space group $P2_12_12$ with one polypeptide chain per asymmetric unit and the following unit cell dimensions: a = 100.1 Å, b = 114.9 Å, and c = 37.8 Å.

Structural Analysis of TcaB9. The initial structure of TcaB9 was determined by multiple isomorphous replacement using three heavy atom derivatives, which were prepared by soaking the crystals in 5 mM potassium gold cyanide, 1.5 mM methylmercury acetate, or 26 mM trimethyllead acetate for 3 days, 2 h, or 5 days, respectively. Prior to X-ray data collection, these crystals were stabilized by transfer to a 1.6 M sodium/potassium phosphate solution (pH 8.0) containing 10 mM dTDP, 5 mM SAM, and 100 mM NaCl. All X-ray data sets for this initial structural analysis were measured at 4 °C using a Bruker HI-STAR area detector system equipped with Supper mirrors. The X-ray source was Cu Kα radiation from a Rigaku RU200 X-ray generator operated at 50 kV and 90 mA. Two gold, four mercury, and three lead binding sites were identified with SOLVE (*10*, *11*), giving an overall figure of merit of 0.61 to 2.5 Å. Solvent flattening with RESOLVE (*11*, *12*) generated an interpretable electron density map, which allowed for a preliminary model of the enzyme to be constructed using COOT (*13*). In the original model, the electron density for SAM was very well ordered, but the electron density corresponding to the nucleotide showed the presence of dTMP rather than dTDP. This structure served as the search model for the subsequent high-resolution structural analyses of TcaB9 complexed with either SAM and dTMP or SAH and dTDP-3-amino-2,3,6-trideoxy-4-keto-3-methyl-D-glucose. The latter structure represents a "product" complex of

Table 1: X-ray Data Collection Statistics[a]

	SAM−dTDP complex	gold derivative	lead derivative	mercury derivative	SAM−dTMP complex	SAH−dTDP-sugar complex
resolution limits	50.2−2.5 (2.6−2.5)	46.8−2.5 (2.6−2.5)	38.4−2.5 (2.6−2.5)	51.1−2.5 (2.6−2.5)	50.5−1.5 (1.6−1.5)	57.2−1.4 (1.5−1.4)
no. of independent reflections	15849 (1558)	15707 (1580)	15873 (1563)	15491 (1426)	68520 (10144)	84778 (14813)
completeness (%)	96.2 (86.6)	96.0 (87.3)	96.8 (87.9)	94.2 (80.3)	96.0 (88.8)	97.4 (94.0)
redundancy	2.5 (1.7)	2.9 (1.9)	2.6 (1.7)	2.4 (1.5)	4.5 (2.5)	4.2 (2.4)
avg I/avg $\sigma(I)$	12.7 (6.2)	13.1 (5.9)	14.2 (6.3)	10.4 (3.8)	10.7 (2.7)	11.1 (2.6)
R_{sym} (%)[b]	6.2 (11.0)	6.1 (11.3)	5.3 (11.1)	7.2 (18.6)	8.4 (35.0)	7.2 (25.4)

[a]Statistics for the highest-resolution bin are given in parentheses. [b]$R_{sym} = (\sum|I - \bar{I}|/\sum I) \times 100$.

Table 2: Model Refinement Statistics

	SAM−dTMP complex	SAH−dTDP-sugar complex
resolution limits (Å)	50.0−1.5	20.0−1.5
R factor[a] (overall) (%)/no. of reflections	19.7/68409	20.5/69883
R factor (working) (%)/no. of reflections	19.5/64961	20.3/66407
R factor (free) (%)/no. of reflections	23.2/3448	24.0/3476
no. of protein atoms	3203[b]	3209[c]
no. of heteroatoms	428[d]	475[e]
average *B* value (Å^2)		
protein atoms	11.0	9.8
metals	10.8	9.6
ligands	6.3[f]	5.5[g]
solvents	22.4	20.9
weighted rms deviations from ideality		
bond lengths (Å)	0.010	0.012
bond angles (deg)	2.1	2.2
general planes (Å)	0.007	0.008

[a]*R* factor = $(\sum|F_o - F_c|/\sum|F_o|) \times 100$, where F_o is the observed structure-factor amplitude and F_c is the calculated structure-factor amplitude. [b]These include multiple conformations for Arg 34, Glu 167, Thr 269, Asp 288, Ser 372, Glu 396, and Arg 414. [c]These include multiple conformations for Glu 22, Asp 39, Arg 149, Thr 152, Arg 165, Asn 298, Asn 355, and Glu 410. [d]Heteroatoms include a dTMP molecule, one metal, two phosphates, a SAM molecule, and 369 waters. [e]Heteroatoms include a dTDP-sugar molecule, one metal, one phosphate, a SAH molecule, and 408 waters. [f]Ligands include SAM and dTMP. [g]Ligands include SAH and dTDP-sugar.

the enzyme. The dTDP-sugar ligand utilized in this investigation was enzymatically synthesized as previously described (*14*).

High-resolution X-ray data sets were collected at 100 K with a Bruker AXS Platinum 135 CCD detector equipped with Montel optics and controlled by the Proteum software suite (Bruker AXS Inc.). These data sets were processed with SAINT version 7.06A (Bruker AXS Inc.) and internally scaled with SADABS version 2005/1 (Bruker AXS Inc.). Prior to X-ray data collection, the crystals were transferred to a solution containing 2.0 M sodium/potassium phosphate (pH 8.0), 5 mM SAM, 10 mM dTMP, 200 mM NaCl, and 15% ethylene glycol. A similar stabilization protocol was employed for the crystals complexed with SAH and dTDP-3-amino-2,3,6-trideoxy-4-keto-3-methyl-D-glucose. Specifically, the crystals were transferred to a synthetic mother liquor containing 1.6 M sodium/potassium phosphate (pH 8.0), 5 mM SAH, and 100 mM NaCl for 4 h to remove the nucleotide. Subsequently, they were transferred to a synthetic mother liquor containing 1.6 M sodium/potassium phosphate (pH 8.0), 5 mM SAH, 15 mM dTDP-linked sugar, and 100 mM NaCl and allowed to soak for 24 h. They were then transferred to a cryoprotectant solution containing 1.95 M sodium/potassium phosphate (pH 8.0), 12.3 mM dTDP-sugar, 3.2 mM SAH, 100 mM NaCl, and 15% ethylene glycol. Relevant X-ray data collection statistics are listed in Table 1.

The structures of the enzyme−dTMP−SAM and the enzyme−SAH−dTDP-sugar complexes were determined via molecular replacement with the software package PHASER (*15*). Refinement with Refmac (*16*) reduced the $R_{working}$ to 19.5 and 20.3% for the models of the enzyme−dTMP−SAM and enzyme−SAH−dTDP-sugar complexes, respectively. Relevant refinement statistics are listed in Table 2.

Measurement of Enzymatic Activity. Enzymatic activity was determined via an HPLC assay. The 4,6-dehydratase (RmlB), the 2,3-dehydratase (EvaA), and the 3-aminotransferase (TcaB8) required for the assay were purified in the laboratory. Reaction mixtures containing 50 mM HEPES (pH 7.5), 100 mM NaCl, 20% glycerol, 20 mM L-glutamate, 2 mg/mL dTDP-glucose, 2 mM SAM, 0.8 mg/mL RmlB, 0.2 mg/mL EvaA, 3 mg/mL TcaB8, and 3 mg/mL TEV-cleaved TcaB9 were incubated at 20 °C, and aliquots were taken to monitor the progress of the reaction as a function of time. For each aliquot, the enzymes were removed via filtration,

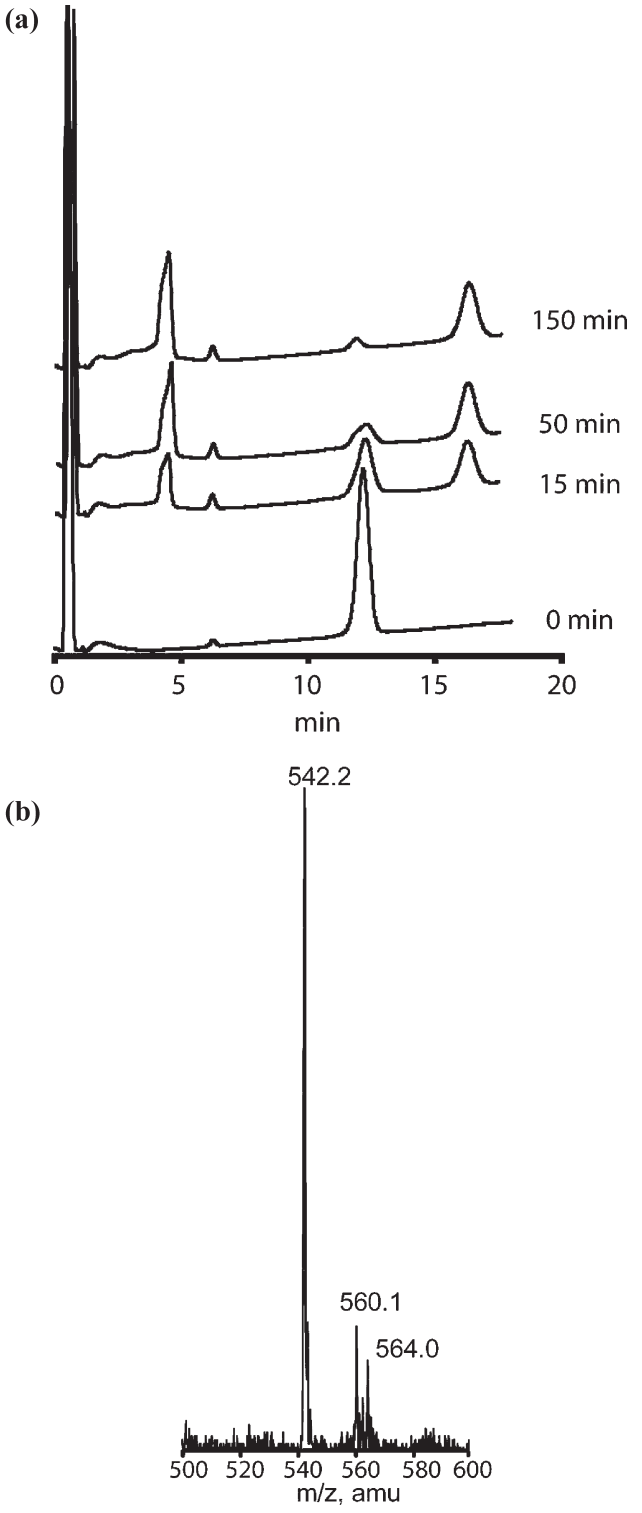

FIGURE 1: Enzymatic activity assay. Shown in panel a is an overlay of HPLC chromatograms corresponding to the 0, 15, 50, and 150 min time points for the TcaB9 activity assay. The mass spectrum shown in panel b is that for the fraction eluting at 4.6 min after the 150 min assay reaction time.

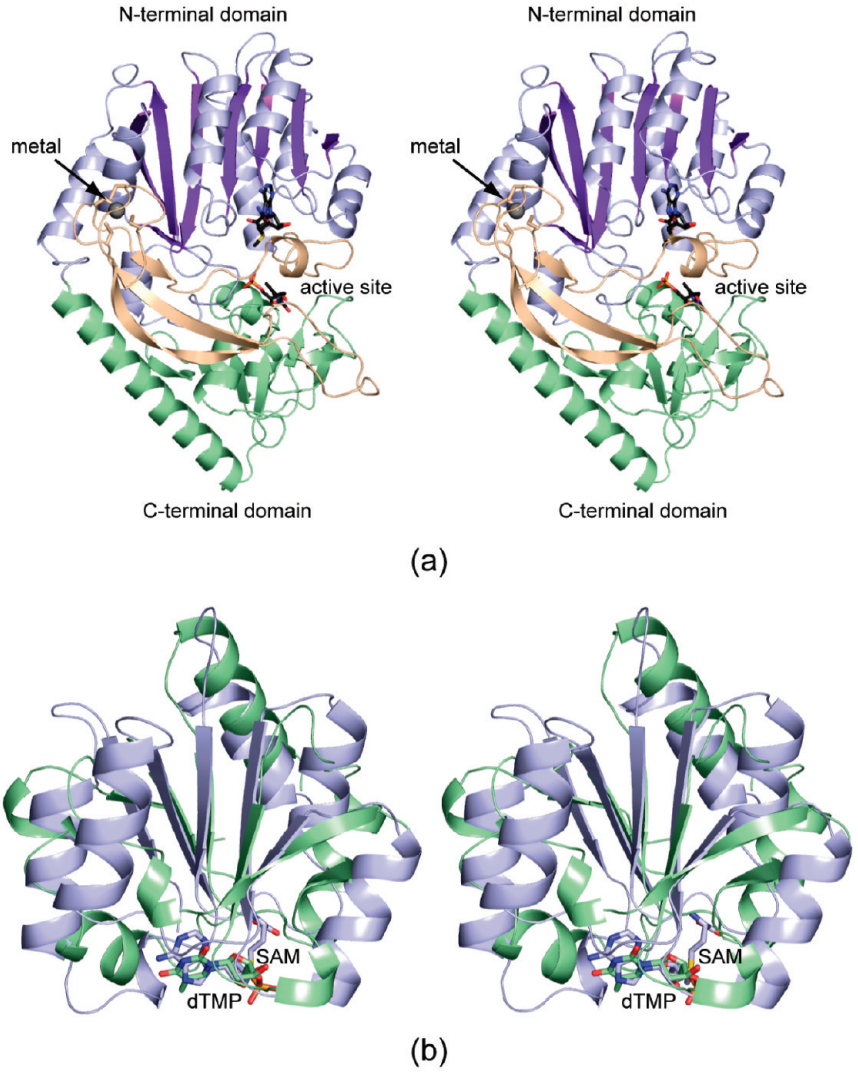

FIGURE 2: Overall structure of TcaB9. A ribbon representation of the enzyme is presented in stereo in panel a. The N-terminal, middle, and C-terminal domains are colored wheat, blue, and green, respectively. Shown in panel b is a superposition of the polypeptide chain from Ala 91 to Asp 206 (blue) and from Arg 303 to Tyr 407 (green). The high degree of structural similarity suggests that the present day form of TcaB9 arose via gene duplication. This figure and Figures 3 and 4 were prepared with PyMOL (*22*).

and the filtrate was diluted 1:9 with water. The various diluted reaction mixtures were analyzed via an AKTA Purifier HPLC system (GE Healthcare) equipped with a 1 mL Resource Q anion exchange column (GE Healthcare) using a 30 mL linear gradient from 0 to 600 mM ammonium acetate (pH 4.0). The products were identified by ESI mass spectrometry.

RESULTS AND DISCUSSION

Enzymatic Activity of TcaB9. Although TcaB9 is annotated as a SAM-dependent *C*-3′-methyltransferase, its actual activity has never been tested (*7*). To verify that it is, indeed, a methyltransferase, reactions were conducted as described in Materials and Methods. At time zero, the HPLC chromatogram showed that SAM and dTDP-glucose elute with retention times of 0.5 and 12.2 min, respectively (Figure 1a). The elution peak corresponding to SAM is present in all of the chromatograms regardless of reaction times. The HPLC chromatograms for the reaction times of 15, 50, and 150 min showed decreases in the magnitudes of the peaks corresponding to dTDP-glucose and the appearance of two new peaks with retention times of 4.6 and 16.7 min. The fractions corresponding to these peaks were subjected to HPLC purification and analyzed by ESI mass spectrometry. Both HPLC controls and ESI mass spectrometry confirmed that dTDP elutes with a retention time of 16.7 min (data not shown). The ESI mass spectrum shown in Figure 1b demonstrates that the fraction eluting with a retention time of 4.6 min corresponds to the TcaB9 product, dTDP-3-amino-2,3,6-trideoxy-4-keto-3-methyl-D-glucose (m/z 542). The peak at m/z 560 in Figure 1b is consistent with the hydrated form of the keto sugar. As further verification of the function of TcaB9, a control reaction was conducted in its absence. Whereas dTDP-glucose was consumed over time (as expected due to the presence of RmlB, EvaA, and TcaB8 in the reaction assay), a peak in the mass spectrum corresponding to the methylated sugar was never observed (data not shown).

Structure of TcaB9 Complexed with SAM and dTMP. In light of both density gradient ultracentrifugation experiments (unpublished data) and crystalline packing, it can be concluded that TcaB9 functions as a monomer. This quaternary structure is similar to that observed for catechol-*O*-methyltransferase (*17*), but in sharp contrast to that of DesVI, a dimeric Class I *N*-methyltransferase that, like TcaB9, functions on nucleotide-linked sugars (*18*).

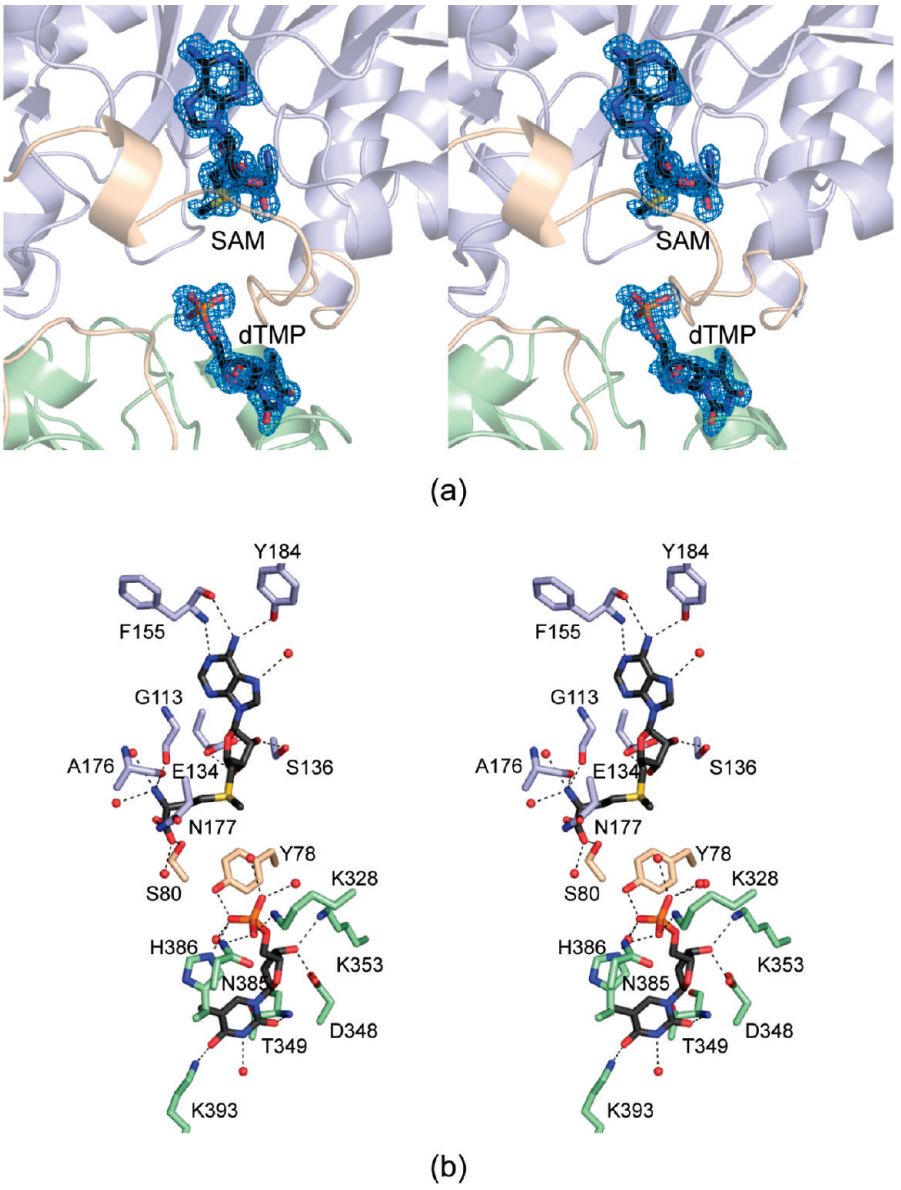

FIGURE 3: Structure of the TcaB9−SAM−dTMP complex. Presented in panel a is an omit map corresponding to the bound ligands. The electron density was contoured at 2.5σ. A close-up view of the active site is displayed in panel b. Amino acid residues contributed by the N-terminal, middle, and C-terminal domains are colored wheat, blue, and green, respectively. Dashed lines indicate distances of ≤3.2 Å. Ordered water molecules are represented as red spheres.

The structure of the TcaB9−SAM−dTMP complex was determined to 1.5 Å resolution. The electron density map was excellent and showed the course of the polypeptide chain from Pro 10 to the C-terminus (Arg 414). Both Pro 374 and Pro 409 adopt *cis*-peptide conformations. These residues are located at the surface of the molecule far removed from the active site cleft. There is only one residue that adopts dihedral angles considerably outside of the allowed regions of the Ramachandran plot, namely Asn 115 (ϕ = 55.4°, and ψ = −137.9°). This residue falls into the "nucleophile" elbow region first described for the α/β-hydrolase family (*19*). Although Asn 115 does not directly interact with the cofactor, it is located near the SAM binding pocket. When this residue is excluded, 92.5 and 7.5% of the ϕ and ψ angles fall within the core and allowed regions of the Ramachandran plot, respectively, according to PROCHECK (*20*).

A ribbon representation of TcaB9 is presented in Figure 2a. The overall fold can be envisioned as three distinct entities: an N-terminal, a middle, and a C-terminal domain. The N-terminal motif, defined by Pro 10−Ser 83, contains three antiparallel β-strands and one small helix. Unexpectedly, the electron density map revealed the presence of a metal, most likely a zinc ion, ligated by Cys 13, Cys 16, Cys 54, and Cys 57 in a tetrahedral arrangement. The metal−ligand bond lengths range from 2.3 to 2.4 Å. The identity of the metal as a zinc is further supported by the observation that TylC3 from the L-mycarose biosynthetic pathway contains approximately 0.4 mol of Zn^{2+}/mol of enzyme (*4*). In the case of TylC3, this metal was shown not to be important for its catalytic activity. The four cysteine residues that ligate the metal are conserved throughout all *C*-3′-methyltransferase amino acid sequences deposited to date (Figure S1 of the Supporting Information).

Following this metal-binding region, the polypeptide chain, defined by Ser 84−Asp 288, folds into a seven-stranded mixed β-sheet flanked on either side by three α-helices. This represents the canonical "SAM-binding" fold. In addition to this fold, the middle domain contains two additional α-helices and an additional

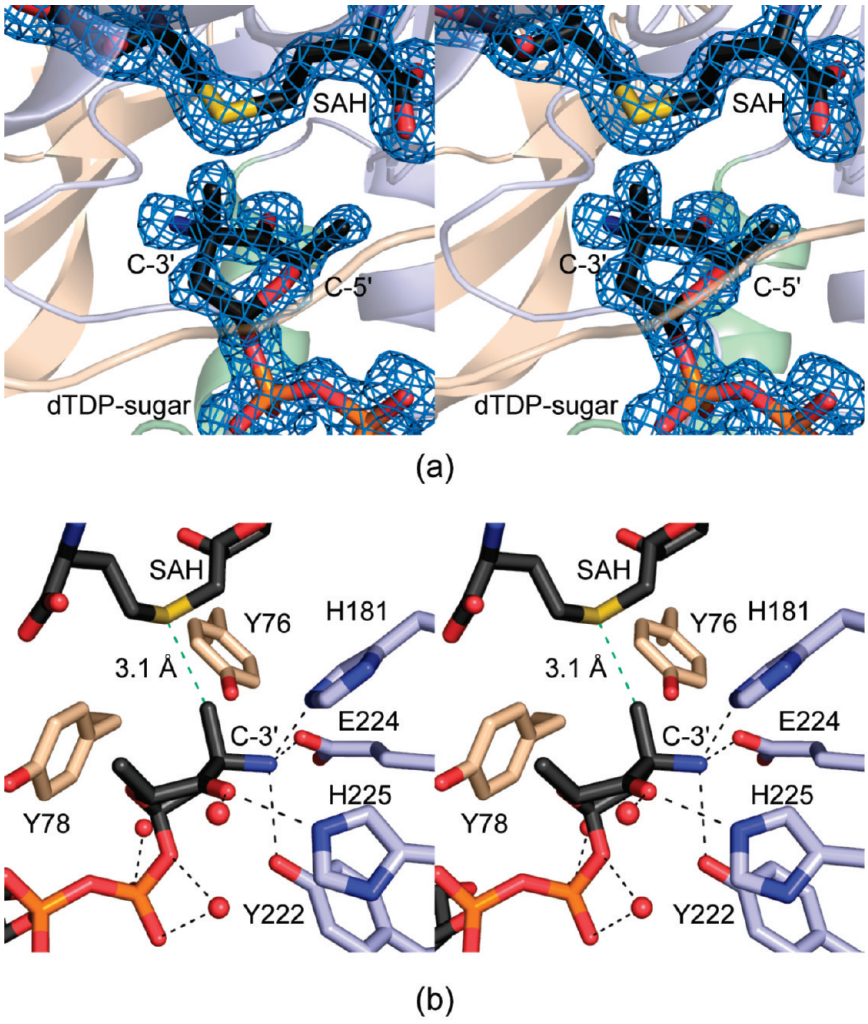

FIGURE 4: Structure of the TcaB9−SAH−dTDP-sugar complex. Presented in panel a is an omit map corresponding to the bound ligands. The electron density was contoured at 2.5σ. A close-up view of the active site is displayed in panel b. Amino acid residues contributed by the N-terminal and middle domains are colored wheat and blue, respectively. Dashed lines indicate distances of ≤3.2 Å. Ordered water molecules are represented as red spheres.

short β-strand (Phe 227−Phe 229) that abuts the third β-strand located in the N-terminal metal binding motif (Figure 2a). The third or C-terminal domain begins at Met 289 with a 27-residue α-helix. After this helix, the polypeptide chain folds into a second seven-stranded β-sheet surrounded by a total of three α-helices. The middle and C-terminal domains appear to be related by an approximate 2-fold rotational axis, suggesting that the present day version of TcaB9 arose via gene duplication. Specifically, Ala 91−Asp 206 align with Arg 303−Tyr 407, leading to a root-mean-square deviation (rmsd) of 3.2 Å for 93 α-carbons. As highlighted in Figure 2b, the first five β-strands of the middle domain overlay with the first five β-strands of the C-terminal domain. The binding positions for the ligands, SAM and dTMP, with respect to the β-sheets are remarkably similar (Figure 2b).

Electron densities corresponding to SAM and dTMP are presented in Figure 3a. All three regions of the enzyme contribute to the binding of these cofactors. The SAM moiety is primarily anchored to the protein via residues contributed by the middle domain. As indicated in Figure 3b, the adenine ring of SAM lies within hydrogen bonding distance of O^{η} of Tyr 184, the backbone amide and carbonyl groups of Phe 155, and a water molecule. Both Glu 134 and Ser 136 interact with the ribose of SAM, with this sugar adopting the $C_{2'}$-*endo* pucker. The backbone carbonyls of Gly 113 and Ala 176, along with two water molecules, hydrogen bond to the amino group of SAM, whereas the carboxylate group of the cofactor lies within 3.2 Å of a water molecule and the side chains of Ser 80 (from the N-terminal domain) and Asn 177. Gly 113 belongs to the characteristic signature sequence referred to as motif I in many SAM-dependent enzymes. In TcaB9, motif I has the following sequence: Ile 109, Val 110, Glu 111, Ile 112, Gly 113, Cys 114, Asn 115, Asp 116, and Gly 117. The dTMP cofactor is positioned in the active site primarily through interactions with residues provided by the C-terminal domain. The thymine ring sits within hydrogen bonding distance of a water molecule, the backbone amide group of Thr 349, and the side chain of Lys 393. Both Asp 348 and Lys 353 hydrogen bond to the C-3 hydroxyl group of the dTMP ribose, which adopts the $C_{2'}$-*endo* pucker. The phosphoryl moiety of dTMP is surrounded by four water molecules, and the side chains of Lys 328, Asn 385, His 386, and Tyr 78 (from the N-terminal domain).

*Structure of TcaB9 Complexed with SAH and dTDP-3-amino-2,3,6-trideoxy-4-keto-3-methyl-*D*-glucose*. The structure of this complex was determined to 1.5 Å resolution, and it represents the "postcatalysis" architecture of the active site. There are very few structural changes in TcaB9 upon dTDP-sugar binding such that the α-carbons for the structures, in the presence

Scheme 2

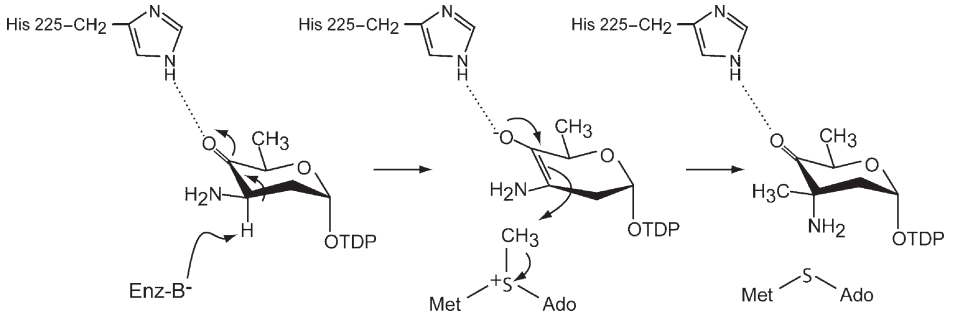

of SAM and dTMP or SAH and dTDP-sugar, correspond with an rmsd of 0.12 Å. Water molecules simply fill the region normally occupied by the sugar. With the exception of Asn 115, 91.7, 8.0, and 0.3% of the ϕ and ψ angles for this product complex lie within the core, allowed, and generously allowed regions of the Ramachandran plot, respectively.

A close-up view of the electron density for the dTDP-linked keto sugar is presented in Figure 4a. The density is very well ordered and, indeed, shows the presence of a keto moiety with its sp^2 hybridization at the C-4′ position. The keto oxygen lies within hydrogen bonding distance of a water molecule and His 225. Three side chains lie within 3.2 Å of the C-3′ amino nitrogen, His 181, Tyr 222, and Glu 224. Amino acid sequence alignments show that these residues are absolutely conserved among the *C*-3′-methyltransferases that function on amino sugars (Figure S1 of the Supporting Information). Both Tyr 76 and Tyr 78 from the N-terminal domain contribute to the binding platform for the sugar. The C-3′ methyl group is 3.1 Å from the sulfur of SAH.

Implications for the Catalytic Mechanism of TcaB9. The first and only *C*-3′-methyltransferase to be kinetically investigated thus far is TylC3 from the L-mycarose biosynthetic pathway (*4*). Its catalytic mechanism is thought to proceed via an enediolate intermediate. According to the proposed mechanism, an enzymatic base abstracts the proton on C-3′ to generate an enediolate, which subsequently attacks the methyl group of SAM. Catalysis by methyltransferases is known to proceed by an S_N2 displacement reaction (*21*). Given that TylC3 and TcaB9 are homologous with a degree of amino acid sequence similarity of 45%, most likely catalysis by TcaB9 proceeds in a similar manner as outlined in Scheme 2. On the basis of the structures presented here, it can be postulated that His 225 plays an important role in stabilizing the enolate intermediate. This residue is strictly conserved among the *C*-3′ sugar methyltransferases (Figure S1 of the Supporting Information). As indicated in Scheme 1, there is a change in configuration about C-3′ upon methylation. The position of the sugar amino group shown in Figure 4b thus serves as a mimic for the location of the hydrogen in the TcaB9 substrate. Three residues lie within 3.2 Å of this nitrogen: His 181, Tyr 222, and Glu 224. Which of these residues functions as the active site base as outlined in Scheme 2 is presently being investigated by site-directed mutagenesis, kinetic experiments, and X-ray crystallographic analyses. Regardless of the identity of the active site base, the structure of this enzyme−SAH−dTDP-sugar complex demonstrates that C-3′ of the nucleotide-linked sugar is, indeed, positioned in the active site for a simple in-line displacement reaction. In addition, the model of TcaB9 described in this report represents a new structural paradigm for *C*-methyltransferases in general.

ACKNOWLEDGMENT

We gratefully acknowledge Professor W. W. Cleland for helpful discussions.

SUPPORTING INFORMATION AVAILABLE

An amino acid sequence alignment of putative *C*-3′-methyltransferases. This material is available free of charge via the Internet at http://pubs.acs.org.

REFERENCES

1. Schubert, H. L., Blumenthal, R. M., and Cheng, X. (2003) Many paths to methyltransfer: A chronicle of convergence. *Trends Biochem. Sci. 28*, 329–335.
2. Martin, J. L., and McMillan, F. M. (2002) SAM (dependent) I AM: The S-adenosylmethionine-dependent methyltransferase fold. *Curr. Opin. Struct. Biol. 12*, 783–793.
3. Thibodeaux, C. J., Melancon, C. E., III, and Liu, H. W. (2008) Natural-product sugar biosynthesis and enzymatic glycodiversification. *Angew. Chem., Int. Ed. 47*, 9814–9859.
4. Chen, H., Zhao, Z., Hallis, T. M., Guo, Z., and Liu Hw, H. (2001) Insights into the branched-chain formation of mycarose: Methylation catalyzed by an (*S*)-adenosylmethionine-dependent methyltransferase. *Angew. Chem., Int. Ed. 40*, 607–610.
5. Thuy, T. T., Lee, H. C., Kim, C. G., Heide, L., and Sohng, J. K. (2005) Functional characterizations of novWUS involved in novobiocin biosynthesis from *Streptomyces spheroides*. *Arch. Biochem. Biophys. 436*, 161–167.
6. Freitag, A., Li, S. M., and Heide, L. (2006) Biosynthesis of the unusual 5,5-gem-dimethyl-deoxysugar noviose: Investigation of the *C*-methyltransferase gene cloU. *Microbiology 152*, 2433–2442.
7. Fang, J., Zhang, Y., Huang, L., Jia, X., Zhang, Q., Zhang, X., Tang, G., and Liu, W. (2008) Cloning and characterization of the tetrocarcin A gene cluster from *Micromonospora chalcea* NRRL 11289 reveals a highly conserved strategy for tetronate biosynthesis in spirotetronate antibiotics. *J. Bacteriol. 190*, 6014–6025.
8. Zhang, H., White-Phillip, J. A., Melancon, C. E., III, Kwon, H. J., Yu, W. L., and Liu, H. W. (2007) Elucidation of the kijanimicin gene cluster: Insights into the biosynthesis of spirotetronate antibiotics and nitrosugars. *J. Am. Chem. Soc. 129*, 14670–14683.
9. Thoden, J. B., Timson, D. J., Reece, R. J., and Holden, H. M. (2005) Molecular structure of human galactokinase: Implications for Type II galactosemia. *J. Biol. Chem. 280*, 9662–9670.
10. Terwilliger, T. C., and Berendzen, J. (1999) Automated MAD and MIR structure solution. *Acta Crystallogr. D55* (Part 4), 849–861.
11. Terwilliger, T. C. (2000) Maximum-likelihood density modification. *Acta Crystallogr. D56* (Part 8), 965–972.
12. Terwilliger, T. C. (2003) Automated main-chain model building by template matching and iterative fragment extension. *Acta Crystallogr. D59*, 38–44.
13. Emsley, P., and Cowtan, K. (2004) Coot: Model-building tools for molecular graphics. *Acta Crystallogr. D60*, 2126–2132.
14. Bruender, N. A., Thoden, J. B., and Holden, H. M. (2010) X-ray structure of kijd3, a key enzyme involved in the biosynthesis of D-kijanose. *Biochemistry 49*, 3517–3524.
15. McCoy, A. J., Grosse-Kunstleve, R. W., Adams, P. D., Winn, M. D., Storoni, L. C., and Read, R. J. (2007) Phaser crystallographic software. *J. Appl. Crystallogr. 40*, 658–674.

16. Murshudov, G. N., Vagin, A. A., and Dodson, E. J. (1997) Refinement of macromolecular structures by the maximum-likelihood method. *Acta Crystallogr. D53*, 240–255.
17. Vidgren, J., Svensson, L. A., and Liljas, A. (1994) Crystal structure of catechol *O*-methyltransferase. *Nature 368*, 354–358.
18. Burgie, E. S., and Holden, H. M. (2008) The three-dimensional structure of DesVI from *Streptomyces venezuelae*: A sugar *N*,*N*-dimethyltransferase required for dTDP-deososamine biosynthesis. *Biochemistry 47*, 3982–3988.
19. Schrag, J. D., and Cygler, M. (1997) Lipases and α/β hydrolase fold. *Methods Enzymol. 284*, 85–107.
20. Laskowski, R. A., MacArthur, M. W., Moss, D. S., and Thornton, J. M. (1993) PROCHECK: A program to check the stereochemical quality of protein structures. *J. Appl. Crystallogr. 26*, 283–291.
21. Bugg, T. (1997) An Introduction to Enzyme and Coenzyme Chemistry, Blackwell Science Ltd., Oxford, U.K.
22. DeLano, W. L. (2002) The PyMOL Molecular Graphics System, DeLano Scientific, San Carlos, CA.